World Journal of Advanced Research and Reviews
eISSN: 2581-9615 CODEN (USA): WJARAI
Cross Ref DOI: 10.30574/wjarr
Journal homepage: https://wjarr.com/

(RESEARCH ARTICLE)

Check for updates

Sub-System Architecture for millimeter-wave massive MIMO systems

Gerald Chukwudi Eze [1,*] and Mamilus Aginwa Ahaneku [2]

[1] *Department of Electronic/Electrical Engineering, Federal Polytechnic, Oko, Aguata, Anambra State, Nigeria.*
[2] *Department of Electronic Engineering, University of Nigeria, Nsukka, Enugu State, Nigeria.*

World Journal of Advanced Research and Reviews, 2024, 22(02), 306–325

Publication history: Received on 16 March 2024; revised on 01 May 2024; accepted on 03 May 2024

Article DOI: https://doi.org/10.30574/wjarr.2024.22.2.1352

Abstract

In this paper, we study the hybrid beamforming design for millimeter-wave (mmWave) massive multiple-input multiple-output (mMIMO) systems. The designing of hybrid beamforming for orthogonal frequency-division multiplexing (OFDM) systems is tasking since its analog beamforming is shared among all subcarriers. We adopt a two-step technique for designing the analog and digital beamforming separately in order to maximize the average achievable energy and spectral efficiency of frequency-selective mmWave mMIMO-OFDM systems. Firstly, the analog beamforming design is based on the viewpoint of sub-systems (SS) and the goal is to optimize the array gain and radio frequency chains. Secondly, the digital beamforming design is carried out by using the regularized channel diagonalization (RCD) and block diagonalization (BD) solutions. On the other hand, the BD solution is modified for single-user. Thus, we propose the use of SS-RCD for multi-user and SS-BD for single-user hybrid beamforming designs. The solutions provide interference suppression but differ in low-SNR performance when communicating to many mobile users via data streams. Simulation results present that our hybrid beamforming design outperforms several other designs.

Keywords: Hybrid beamforming; Sub-system; Block diagonalization; Regularized channel diagonalization; Millimeter-wave; Massive MIMO-OFDM.

1. Introduction

The future generation wireless networks will promote and enhance new technologies such as smart environments, augmented and virtual reality, industrial and agricultural automation, and autonomous vehicles [1]. Increased connectivity, higher capacity, and lower latency are the stringent requirements for new technologies [2], forcing telecommunication operators to migrate to higher frequency bands, such as millimeter-wave (mmWave) and terahertz (THz) frequencies [3]. Moreover, such high frequencies are mainly affected by penetration loss, atmospheric attenuation and path loss. Therefore, THz and mmWave networks will rely on massive multiple input multiple output (mMIMO) to lessen the effects of unfavorable propagation and to give additional spatial multiplexing gains and diversity [4]. Nonetheless, the increasing cost of power consumption and radio-frequency (RF) chains, especially at high frequencies, will make it impractical to implement fully-digital beamforming in mMIMO networks [5].

Hence, hybrid digital and analog beamforming (BF) is a major key to enable mMIMO in mmWave and THz communications [6–8]. Hybrid beamforming (HBF) is a combination of a reduced-dimension digital beamforming and a high-dimensional analog beamforming, connected by a small number of RF chains. To enjoy the gains of digital beamforming and analog beamforming, the fully adaptive connected HBF structure is proposed for improving the energy efficiency (EE) of the network [9]. In [9], authors designed a matching assisted fully adaptive hybrid precoding (MA-FAHP) algorithm to jointly optimize the analog and digital beamforming as well as the connection state matrix for enhancing the EE.

* Corresponding author: Gerald Chukwudi Eze

1.1. Related works

The large-scale antenna arrays (LSAA) for HBF was investigated in [10] and [11]. In [10], authors considered HBF design for orthogonal frequency-division multiplexing (OFDM)-based systems with LSAA. The authors presented that the HBF structure is an appropriate scheme for broadband mmWave systems with frequency selective channels. Particularly, for single user (SU) MIMO systems, authors presented that the HBF structure can asymptotically achieve the optimal fully-digital beamforming for sufficiently large number of antennas. In [11], authors presented that HBF structure can realize the same performance of any fully digital beamforming scheme with much fewer number of RF chains; the needed number RF chains only requires to be twice the number of data streams. Supported by the LSAA, the reduced number of RF chains and multiplexing gains of mMIMO, HBF structures give near-optimal performance with increased EE and hardware complexity [5]. To reduce the number of RF chains, the HBF structure has been proposed to overcome this challenge [10–11, 35], where the digital beamforming and analog beamforming are fulfilled by phase shifters (PS) and the RF chains, respectively. The coupling between the analog beamforming and digital beamforming, as well as the constant modulus constraint imposed by the PS, via which the analog beamforming is implemented, result in non-linear, non-convex, and often intractable design problems [12].

Prior literature works on HBF design focused on utilizing the mmWave sparse-scattering channels to formulate the HBF design based on sparsity constrained matrix reconstruction problem. The researchers sought by disconnecting the combiner and precoder design separately, the problem can be cast as an approximation problem that minimizes the Frobenius norm of the difference between finding for the best projection of the optimal unconstrained beamforming onto the set of feasible HBF [23]. The problem made up of a matrix-factorization problem and the solution is found by using the compressive-sensing-based algorithms. By the inspiration of the same matrix-factorization problem, the authors in [13] proposed two alternating-minimization (AltMin) techniques for HBF designs with major focus on phase-extraction (PE) and manifold optimization (MO). The PE-based design trades off a slight performance loss for a lower computational complexity while the MO-based design can achieve near-optimal performance, but its computational complexity limits its practical implementation. In spite of the performance loss in PE-based design, the PE-AltMin algorithm out performs most of the currently existing algorithms.

On the other hand, the promising results achieved for narrowband networks, researchers had begun to explore frequency selective broadband channels, considering, especially, OFDM networks because of large bandwidths available in mmWave and THz. The OFDM permits decomposition of the broadband channel into multiple non-interfering frequency-flat narrowband channels with independent subcarriers; the analog beamforming is distributed among all these subcarriers, therefore making design of the HBF-OFDM ever more difficult [13-16]. Recently, the design of HBF-OFDM for SU-MIMO systems was studied in [10-14], while the design of HBF-OFDM for multi-user (MU) MIMO systems were investigated in [15-16, 19] with multi-stream transmission.

Finally, the authors in [14] proposed the sub-system (SS) singular value decomposition (SVD) HBF design for SU and studied OFDM-MIMO systems over mmWave channels under practical HBF constraints that analog beamformers are fixed for all subcarriers. Authors of [14] designed the sub-systems HBF which requires no iterative operations for SU. Numerical results present that SS algorithm gives the performance of conventional full-digital beamforming with low complexity.

In this paper, we design and study HBF for SU and MU MIMO-OFDM systems over mmWave channels based on the viewpoint of SS, we first use a low-complexity HBF design without iterative computations between analog combiner and precoder. At the first stage, a SS representation of the OFDM channel is used to formulate the analog beamforming design as unconstrained SVD problem. At the second stage, the digital combiner and precoder for SU systems are obtained from the optimal block diagonalization (BD) solution [17-18], considering the digital baseband. For MU systems, the digital beamforming is achieved using the regularized channel diagonalization (RCD) solution [19]. This problem formulation allows maximizing the sum of the effective baseband gains over every subcarrier while nulling both multi-user interference (MUI) and intra-user interference (IUI) within the same subcarrier.

The main contributions of this paper are designing a SS for MU MIMO-OFDM, combination of SS either with RCD or BD to maximize the Energy and Spectral Efficiencies of mm-Wave mMIMO system, the expansion of SS-SVD HBF design from SU to MU, and modification of BD for SU.

2. System model and problem formulation

In this section, we present the system model, followed by the channel model and the problem formulation.

2.1. System Model

Here, we consider the mMIMO-OFDM system with a HBF structure. The system block diagram is depicted in Fig. 1. It is assumed that a base station having number of transmitted antennas N_T and RF transmitting chains N_T^{RF} simultaneously communicates with K mobile users via number of subcarriers M. Each user is equipped with number of received antennas N_R and RF receiving chains N_R^{RF} and supports number of data streams N_S per subcarrier. To ensure effective multi-stream communication, the system must satisfy $N_S \leq N_R^{RF} \leq N_R$ and $KN_S \leq N_T^{RF} \leq N_T$ [10–11]. At the base station, the hybrid precoder consists of digital precoder matrix $F_{BB} = [F_{BB,1} \dots F_{BB,k} \dots F_{BB,K}] \in \mathbb{C}^{N_T^{RF} \times KN_S}$ where $F_{BB,k} \in \mathbb{C}^{N_T^{RF} \times N_S}$ is the digital precoder matrix for the k-th user and the analog precoder matrix $F_{RF} \in \mathbb{C}^{N_T \times N_T^{RF}}$. The analog precoder is implemented using phase shifters and is subjected to a constant modulus constraint (i.e. $|F_{RF}(m,n)| = 1\sqrt{N_T}$ all m, n). The symbol vector s = $[s_1^T, s_2^T, \dots s_K^T] \in \mathbb{C}^{1 \times KN_S}$, where $s_k^T \in \mathbb{C}^{1 \times N_S}$ refers to the k-th user's symbols, is assumed independent with unity-variance components, i.e. $\mathbb{E}[ss^H] = I_{KN_S}$, and is precoded in the digital and analog domains before being transmitted, yielding the following transmitted signal

$$x = F_{RF}F_{BB}s \tag{1}$$

where $x \in \mathbb{C}^{N_T \times 1}$ and we assuming that the signal is transmitted over a narrowband flat-fading channel $H_{m,k} \in \mathbb{C}^{N_R \times N_T}$, where $H_{m,k}$ represents the fast-fading channel matrix for the m-th subcarrier and the k-th user, the signal received at k-th user's antenna array, $y_k \in \mathbb{C}^{N_R \times 1}$ is given by

$$y_k = \sqrt{\alpha}H_{m,k}F_{RF}F_{BB}s + n_k \tag{2}$$

Where α represent the large scale fading and $n_k \in \mathbb{C}^{N_R \times 1}$ is the noise vector.

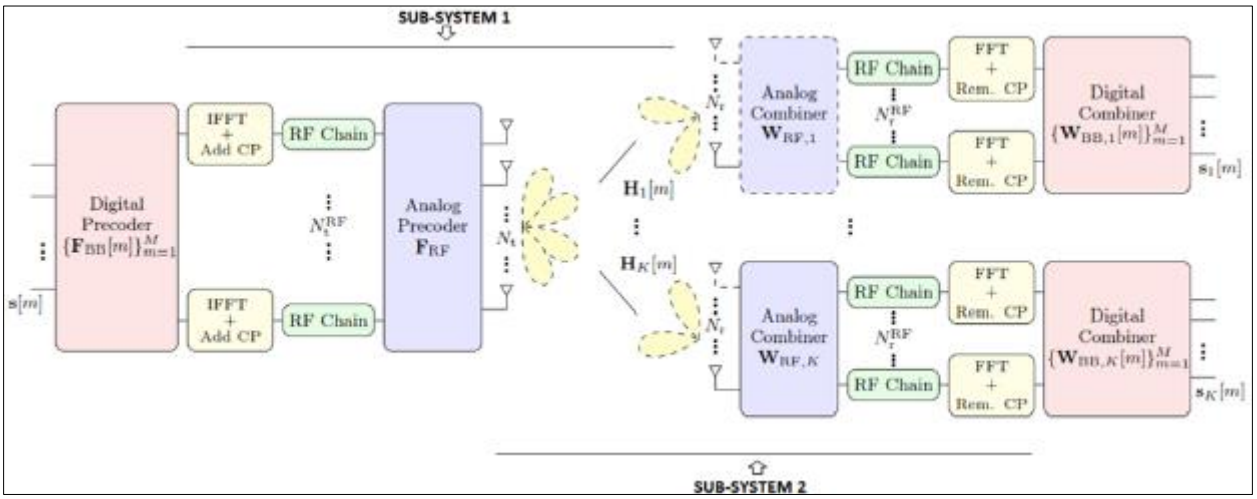

Figure 1 Overall MU-MIMO-OFDM system with HBF architecture and sub-systems block diagram [14, 27-28].

The symbols then go via the digital precoder refer to as OFDM modulation, where the cyclic prefix (CP) and the inverse fast Fourier transform (IFFT) operations take place, assuming that the cyclic CP's length is large enough to prevent inter-carrier-interference (ICI) [20]. The modulated symbols are then precoded on the analog domain using the analog precoder common to all subcarriers. The sub-system 1 contains the IFFT, CP additional, analog precoder and mmWave channel [14].

At the k-th user, the received signal y_k is first processed by the analog combiner matrix $W_{RF,k} \in \mathbb{C}^{N_R \times N_R^{RF}}$, and secondly, processed by the digital combiner matrix $W_{BB,k} \in \mathbb{C}^{N_R^{RF} \times N_S}$. The analog combiner is also implemented using PSs and is constrained to have a constant modulus, such that $|W_{RF}(m,n)| = 1\sqrt{N_R}$ (all m, n). The received symbol is expressed by

$$\dot{s}_k = \sqrt{\alpha}W_{BB,k}^H W_{RF,k}^H y_k \tag{3}$$

By defining the aggregated multiuser channel as H = $[H_1^T\ H_2^T\ \dots\ H_K^T\ ]^T$, the aggregated analog

combining matrix as $W_{RF} = \text{blkdiag}\{W_{RF,1} \dots W_{RF,K}\}$, , and the effective baseband channel of the k-th mobile user as $H_{eff} = W_{RF,k}^H H_{m,k} F_{RF} \in \mathbb{C}^{N_R^{RF} \times N_T^{RF}}$, we can represent the entire multiuser effective baseband channel H_{eff} as $H_{eff} = W_{RF,k}^H H_{m,k} F_{RF}$.

$$H_{eff} = \begin{bmatrix} W_{RF,1}^H & 0 & \dots & 0 \\ 0 & W_{RF,2}^H & \cdots & \vdots \\ \vdots & \vdots & \ddots & \\ 0 & 0 & \dots & W_{RF,K}^H \end{bmatrix} \begin{bmatrix} H_1 \\ H_2 \\ \vdots \\ H_K \end{bmatrix} F_{RF} \tag{4}$$

The estimated symbol for the i-th data stream in the k-th user, $\dot{s}_k$, can be expressed as

$$\dot{s}_k = \sqrt{\alpha} W_{BB,k}^H(i,:) \bar{H}_{m,k} F_{BB}(:,k_i) s_{k_i} + \sum_{j=1, i \neq j}^{N_S} \sqrt{\alpha}\, W_{BB,k}^H(i,:) \bar{H}_{m,k} F_{BB}(:,k_j) s_{k_j}$$

$$+ \sum_{m=1, m \neq k}^{K} \sum_{j=1}^{N_S} \sqrt{\alpha}\, W_{BB,k}^H(i,:) \bar{H}_{m,k} F_{BB}(:,m_j) s_{m_j} + W_{BB,k}^H(i,:) W_{RF,k}^H n_k \tag{5}$$

where $k_i = (k-1)N_S + i$ and s_{k_i}, is the i-th element of s_k. The signal then goes through the digital combiner known as OFDM demodulation, which applies the fast Fourier transform (FFT) and the CP removal operations. The demodulated signal is finally combined in the digital domain via the combining matrix $W_{BB,k}[m]$ on a per-subcarrier basis. The sub-system 2 contains the FFT, CP removal, analog combiner and mmWave channel [14].

2.1.1. Performance measures

Two performance measures considered are the spectral efficiency (SE) and the energy efficiency (EE). The SE is measured in (bits/s/Hz) while the EE is measured in (bits/Hz/J). The achieved spectral efficiency (SE) for m-th subcarrier is given by [21]

$$SE = \frac{1}{M} \sum_{k=1}^{K} \sum_{m=1}^{M} \log_2 \left(\left| I_{N_S} + \frac{\alpha}{\sigma^2} R_N^{-1} W_k^H H_k F_k F_k^H H_k^H W_k \right| \right) \tag{6}$$

where $F_k \triangleq F_{RF} F_{BB,k}$, $W_k \triangleq W_{RF} W_{BB,k}$, and $R_N = \frac{\alpha}{\sigma^2} \sum_{j \neq k}^{K} W_k^H H_k F_j F_j^H H_k^H W_k + W_k^H W_k$ is the interference plus noise covariance matrix. The EE is defined as

$$EE = \frac{W \times SE}{\eta \sum_1^K \sum_1^{N_S} p_{k,q} + P_{TX} + K P_{RX}} \tag{7a}$$

$$\sum_1^K \sum_1^{N_S} p_{k,q} = K N_S = P_T$$

where $p_{k,q}$ is the power allocated to the N_S-th data stream and k-th user, W is the system bandwidth, P_{TX} is the amount of power consumed by the transmitter circuitry, P_{RX} is the amount of power consumed by the receiver circuitry, P_T is the transmit power, and η>1 is a scalar coefficient modeling the Power Amplifier (PA) inefficiency [22]. The cost due to signal processing at both the transmitter and the receiver is contained in the terms P_{TX} and P_{RX} which will be specified later for each HBF structure. The P_{TX} can therefore be expressed as

$$P_{TX} = N_T (P_{RFC} + P_{DAC} + P_{PA}) + P_{BB} \tag{7b}$$

and the P_{RX} can be expressed as

$$P_{RX} = N_R (P_{RFC} + P_{ADC} + P_{LNA}) + P_{BB} \tag{7c}$$

where P_{RFC} is the power consumed by the single RF chain, P_{DAC} is the power consumed by each digital analog converter (DAC), P_{ADC} is the power consumed by each analog digital converter (ADC), P_{PA} is the power consumed by each PA, P_{LNA} is the power consumed by each low noise amplifier (LNA), and P_{BB} is the amount of power consumed by each baseband precoder or combiner [22].

2.2. Channel model

The Saleh-Valenzuela channel model is considered and it represents the sparse scattering environment of mmWave channels unlike the Rayleigh model, which represents a rich scattering environment. The Saleh-Valenzuela channel model is a fast fading channel model and corresponds to the sum of the contributions of N_{cl} scattering clusters, each formed by N_{ray} propagation paths plus a possibly present line-of-sight (LoS) component. The baseband equivalent of the propagation channel between the base station and the k-th mobile user is therefore represented by an ($N_R \times N_T$)-dimensional matrix expressed as

$$H_{m,k} = \gamma \sum_{i=0}^{N_{cl}-1} \sum_{l=0}^{N_{ray}-1} \rho_{il} a_R(\varphi_{il}^R, \vartheta_{il}^R) a_T^H(\varphi_{il}^T, \vartheta_{il}^T) e^{j\frac{-2\pi i(m-1)}{M}} + H_{LoS} \quad (8a)$$

where ρ_{il} denotes the complex gain of the l-th multipath ray in the i-th cluster, the vectors $a_R^H(\varphi_{il}^R, \vartheta_{il}^R)$ and $a_T^H(\varphi_{il}^T, \vartheta_{il}^T)$ are the array response vectors of the receiver and transmitter, respectively, whereas the parameters φ_{il}^T and ϑ_{il}^T denote the azimuth and elevation angles of departure (AoD), and the parameters φ_{il}^R and ϑ_{il}^R denote the azimuth and elevation angles of arrival (AoA). The complex gain ρ_{il} is considered to be i.i.d. $\mathcal{CN}(0, \sigma^2)$ where σ^2 is the average power of the i-th cluster and $\gamma = \sqrt{N_R N_T / N_{cl} N_{ray}}$ is the normalization factor [21].

The average cluster powers are such that $\sum_{i=1}^{N_{cl}} \sigma^2 = \sqrt{N_R N_T / N_{cl} N_{ray}}$ [23]. The azimuth and elevation angles of departure ($\varphi_{il}^T \vartheta_{il}^T$) and arrival ($\varphi_{il}^R \vartheta_{il}^R$) for the N_{ray} paths in the i-th cluster are modeled as Laplacian distributed random variable, with mean $\varphi_{il}^T, \vartheta_{il}^T, \varphi_{il}^R, \varphi_{il}^R$ uniformly-distributed over $[-\pi, \pi)$, and angular spread of $\sigma_\varphi^T, \sigma_\varphi^R, \sigma_\vartheta^T, \sigma_\vartheta^R$ respectively. A $\sqrt{N} \times \sqrt{N}$ uniform square planar array (USPA) is considered with $N = N_T$ for the transmitter or $N = N_R$ for the receiver. The array response vector for the USPA is defined as [24]

$$a(\varphi, \vartheta) = \frac{1}{\sqrt{N}} \left[1, \dots, e^{j\frac{2\pi d}{\lambda}[h \sin\varphi \sin\vartheta + v \cos\vartheta]}, \dots, e^{j\frac{2\pi d}{\lambda}[(\sqrt{N}-1)\sin\varphi \sin\vartheta + (\sqrt{N}-1)\cos\vartheta]}\right]^T \quad (8b)$$

where d and λ denote the spacing between elements and the signal wavelength, respectively, and $0 < h < (\sqrt{N} - 1)$ and $0 < v < (\sqrt{N} - 1)$ represent the indexes of the antenna element in the 2D plane. Focusing on the LoS component, representing by $\varphi_{LoS}^T, \varphi_{LoS}^R$ the departure and arrival angles corresponding to the LoS link, it is considered that:

$$H_{LoS} = I_{LoS}(d) \sqrt{N_R N_T L(d)} a_R(\varphi_{LoS}^R) a_T^H(\varphi_{LoS}^T) e^{j\vartheta} \quad (8c)$$

where $L(d)$ is the attenuation associated to the propagation distance, and I_{LoS} is a random variate indicating if an LoS link exists between transmitter and receiver, with the probability that $I_{LoS} = 1$, that is an LoS exists[21].

2.3. Problem formulation

Here, the design of hybrid precoders and combiners aims to maximize the EE of mm-Wave mMIMO system. This design problem is formulated as

$$\max_{F_{RF}, W_{RF}} \frac{W \times SE}{\eta K N_S + P_{TX,c} + K P_{RX,c}}$$

$$\text{Subject to} \quad \begin{aligned} &F_{RF} \in \mathcal{F}_{RF} \\ &W_{RF} \in \mathcal{W}_{RF} \\ &\|F_{RF} F_{BB}\|_F^2 = P_T. \end{aligned} \quad (9)$$

Where $\mathcal{F}_{RF}$ and $\mathcal{W}_{RF}$ are, respectively, the set of all feasible analog precoder and combiner matrices (i.e., all $N_T \times N_T^{RF}$ and $N_R \times N_R^{RF}$ matrices with constant modulus entries), and $\|F_{RF} F_{BB}\|^2 = P_T$ ensures the total transmitted power constraint. For simplicity, it is assumed that

$$N_T^{RF} = K N_R^{RF} = K N_S . \quad (10)$$

2.4. Proposed HBF Design

2.4.1. Sub-System (SS) Design

In this section, our HBF design is based on the viewpoint of sub-systems (SS). Channel state information (CSI) is assumed to be known perfectly at the base station, $H_{m,k}$ for m = 1, 2 … M and k = 1, 2 … K is available. In our HBF design, we derive analog beamformers by studying SS of the overall system. Consider the sub-systems block illustrated in Fig. 1. The sub-systems block regards s_k as the system input and y_k as the system output.

Conventional full-digital beamforming which obtains the maximum of (5) is based on singular value decomposition (SVD) of the channel matrix with water-filling power allocation. This method considers that each antenna is connected to a complete RF chain, which is expressed in [14] with the analog precoder and the analog combiner with $N_T^{RF} = N_T$ and $N_R^{RF} = N_R$ respectively. Then the maximization of achievable rate sub-systems of analog precoder and the analog combiner in [14] implies that analog precoder and the analog combiner can be found from SVD of

$$H_{S1} = \sum_{k=1}^{K} \sum_{m=1}^{M} H_{m,k}^H H_{m,k}$$

$$F_{RF,k} = \frac{U_{S1}}{|U_{S1}|} \tag{11}$$

Let $H_{S1} = U_{S1} W_{S1} V_{S1}^H$ by SVD. The unconstrained analog precoder $F_{RF,k} \in \mathbb{C}^{N_T \times N_T^{RF}}$.

$$H_{S2} = \sum_{k=1}^{K} \sum_{m=1}^{M} H_{m,k} H_{m,k}^H$$

$$W_{RF,k} = \frac{U_{S2}}{|U_{S2}|} \tag{12}$$

Let $H_{S2} = U_{S2} W_{S2} V_{S2}^H$ by SVD. The unconstrained analog combiner $W_{RF,k} \in \mathbb{C}^{N_R \times N_R^{RF}}$.

Authors in [14] investigated SS-OFDM-MIMO systems over mmWave channels for SU without considering MU. In this paper, the SS-SVD is expanded from SU to MU using both (MU-SS) algorithm and (MU-SVD) algorithm shown below. Note that our HBF design only has to find the matrices H_{S1} and H_{S2}, for all k, and compute SVD of these matrices once without iterative operations.

Algorithm 1: Multi-user subsystems (MU-SS)

1 **Input:** $H_{m,k}(N_R, N_T)$, N_T^{RF}, N_R^{RF}, M, K

2 **Analog Precoder Design on Sub-system 1:**

$$H_{S1} = \sum_{k=1}^{K} \sum_{m=1}^{M} H_{m,k}^H (N_R, N_T) H_{m,k}(N_R, N_T)$$

3 **Analog Combiner Design on Sub-system 2:**

$$H_{S2} = \sum_{k=1}^{K} \sum_{m=1}^{M} H_{m,k}(N_R, N_T) H_{m,k}^H (N_R, N_T)$$

4 **Perform Singular Value Decomposition of H_{S1} & H_{S2}:**

$$[U_{S1}\ W_{S1}\ V_{S1}] = \text{SVD}\ (H_{S1})$$
$$[U_{S2}\ W_{S2}\ V_{S2}] = \text{SVD}\ (H_{S2})$$

5 **Set Analog Precoder:**

$$F_{RF}(N_T, N_T^{RF}) = \frac{U_{S1}(N_T, 1{:}\, N_T^{RF})}{|U_{S1}(N_T, 1{:}\, N_T^{RF})|}$$

6 **Set Analog Combiner:**

$$W_{RF}(N_R, N_R^{RF}) = \frac{U_{S2}(N_R, 1{:}\, N_R^{RF})}{|U_{S2}(N_R, 1{:}\, N_R^{RF})|}$$

7 **Output:** $F_{RF}(N_T, N_T^{RF}), W_{RF}(N_R, N_R^{RF})$

Algorithm 2: Multi-user Singular Value Decomposition (MU-SVD)

Input: $H_{m,k}(N_R, N_T)$, $F_{RF}^{opt}(N_T, N_T^{RF})$, $W_{RF}^{opt}(N_R, N_R^{RF})$, N_S, M, K
Digital Combiner and Precoder Design:
For k = 1: K do
  For m = 1: M do
    $H_{EFF} = W_{RF}^{opt\,H} \times H_{m,k}(N_R, N_T) \times F_{RF}^{opt}$
    Perform Singular Value Decomposition of H_{EFF}:
    $[U_E W_E V_E]$ = SVD (H_{EFF})
    $W_{BB,m,k}(N_R^{RF}, N_S) = U_E(:, 1{:}N_S)$
    $W_{BB,m,k}(N_T^{RF}, N_S) = W_{RF}^{opt}(N_R, N_R^{RF}) \times W_{BB,m,k}(N_R^{RF}, N_S)$
    $F_{BB,m,k}(N_T^{RF}, N_S) = \sqrt{P_t} \times \frac{V_E(:,1:N_S)}{\|F_{RF}(N_T, N_T^{RF}) \times V_E(:,1:N_S)\|_F}$
    $F_{m,k}(N_T, N_S) = F_{RF}^{opt}(N_T, N_T^{RF}) \times F_{BB,m,k}(N_T^{RF}, N_S)$
  End
End
Output: $F_{m,k}(N_T, N_S)$, $W_{m,k}(N_R, N_S)$

2.4.2. Digital Precoder and Combiner Design

We propose a combination of SS and RCD methods for HBF design for OFDM systems. At the first stage, we design the analog precoders and combiners using SS approach i.e., Algorithm 1 for both SU and MU. For the MU scenario, we adopt the RCD method for designing the digital precoder and combiner [19, 28]. On the other hand, FDBD approach [17-18] is modified for SU scenario, which is designed to minimize only the IUI, the RCD aims to suppress the MUI plus noise. As a result, the RCD can give higher transmit diversity and high performance in low-SNR scenarios or when there is large data streams or number of mobile users.

Regularized block diagonalization-based fully digital (FDRBD) solution

First, consider a MU system (i.e., $K \neq 1$), where interference is present. In this case, for a given analog combiner and precoder matrix, the optimal digital combiner and precoder matrices are achieved from the effective baseband channel's FDRBD, followed by the water-filling power allocation [25].The effective baseband channel, i.e., $H_{eff}^{(k)} = W_{RF,k}^H H_{m,k} F_{RF,k}$, takes into account the effects of the analog combiner and precoder.

$$\widetilde{H}_k = [H_{eff}^{(1)} \ \dots \ H_{eff}^{(k-1)} H_{eff}^{(k+1)} \ \dots \ H_{eff}^{(K)}]^T \tag{13}$$

where $\widetilde{H}_k \in \mathbb{C}^{(K-1)N_R \times N_T}$. Based on the obtained baseband equivalent channel $\widetilde{H}_k$, given the found RF processing matrices F_{RF}, we perform the low-dimensional RBD processing with the baseband precoder F and combiner W to cancel the interference. To obtain the primary baseband precoder as given by [17-18]

$$F_a = \left(\widetilde{H}_k^H \widetilde{H}_k + \frac{KN_S\sigma^2}{P_T} I_{N_T}\right)^{-1} \tag{14}$$

Given the above results, FDRBD of the baseband equivalent channel matrix to remove user interference is written as

$$H_{FDRBD} = \widetilde{H}_k F_a = U_s \Sigma_s V_s^H \tag{15a}$$

Since the resulting multiplication of baseband equivalent channel and primary baseband precoder (i.e. $\widetilde{H}_k F_a$) will be regularized block diagonal, the method is referred to here as RBD [18]. The secondary baseband precoder is the $F_b = V_s$. The FDRBD baseband combiner is $W = U_s$ and the FDRBD baseband precoder is obtained as

$$F = \sqrt{\frac{P_T}{K}} \times F_a \times F_b / \|F_a F_b\|_F \tag{15b}$$

For block diagonalization-based fully digital (FDBD) solution, FDBD is modified for SU system (i.e., $K = 1$), let $H_k = H_{eff}^{(k)}$, the primary baseband precoder is extracted from the SVD of $H_k = W_a \Sigma_a F_a^H$ and viewed as optimizing K parallel SU. Here the resulting multiplication of H_k and F_a will be block diagonal, the method is known as BD [33].

$$H_{FDBD} = H_k F_a = U \Sigma V^H \tag{16a}$$

The secondary baseband precoder is the $F_b = V$. The BD baseband combiner is $W = U$ and the BD baseband precoder is obtained as

$$F = \sqrt{\frac{P_T}{K}} \times F_a \times F_b / \|F_a F_b\|_F \tag{16b}$$

The digital primary precoder makes the k-th user to transmit in the null-space of $\widetilde{H}_k$, thereby producing a better MUI mitigation [17-18, 33].

Regularized channel diagonalization (RCD) solution

In contrast to the RBD, that only focuses on the MUI, the RCD technique can trade-off MUI reduction for noise reduction and transmit diversity, therefore obtaining a better performance in low-SNR regimes. Unlike SU systems, where the precoders and combiners are designed to increase the effective gain and reduce interference (i.e., IUI), MU systems also require to address noise and inter-user interference (i.e., MUI). Besides, in SU systems, the optimal EE can be attained using linear processing. Here, the RCD approach is adopted to design the digital precoder and combiner. The RCD's aim is to reduce the interference plus noise and to optimize the system performance. Therefore, the RCD design is achieved in two stages: the first step addresses the MUI plus noise suppression, and the second step performs the IUI suppression and performance optimization. The digital precoder is expressed as

$$F_{BB}[m] = \beta F_a[m]F_b[m] \tag{17}$$

where β is is selected to ensure the total transmit power constraint (9), the primary precoder $F_a[m] = [F_{a1}[m]\ F_{a2}[m] \dots F_{aK}[m]] \in \mathbb{C}^{KN_S \times KN_S}$ is intended for MUI and noise suppression, and the secondary precoder $F_b[m] = diagonal\ [F_{b1}[m]\ F_{b2}[m] \dots F_{bK}[m]] \in \mathbb{C}^{KN_S \times KN_S}$ performs IUI suppression and performance optimization. Given that the k-th user's digital equivalent channel $\ddot{H}_k^{eq} = W_k^H H_{mk} F$ and $F_{ak}[m] \in \mathbb{C}^{KN_S \times N_S}$ is given by [19, 28]

$$F_{ak} = \left(\ddot{H}_k^H \ddot{H}_k + \frac{KN_S\sigma^2}{P_T} I_{KN_S}\right)^{-1} \tag{18}$$

where $\ddot{H}_k = \left[\ddot{H}_1^{eq} \dots \ddot{H}_{k-1}^{eq} \ddot{H}_{k+1}^{eq} \dots \ddot{H}_K^{eq}\right]^T \in \mathbb{C}^{(K-1)N_S \times KN_S}$ is the digital baseband channel with corresponding reduced rank channel which removes the k-th user's digital equivalent channel [19]. The formulation of digital precoder design problem is investigated and explained in [19]. The SU-MIMO digital effective channel for the k-th user is $\ddot{H}_k F_{ak}$ and SVD of $\ddot{H}_k F_{ak} = U_s \Sigma_s V_s^H$. The secondary precoder $F_{bk}[m] = V_s \in \mathbb{C}^{N_S \times N_S}$ and the digital combiner $W_{BB} = U_s$, designed to suppress IUI and further optimize the system's performance. The baseband precoder is $F = F_{RF} F_{BB}$ and baseband combiner is $W = W_{RF} W_{BB}$. The digital primary precoder makes the k-th user transmits in the subspace spanned by all other users with power inversely proportional to $\ddot{H}_k$'s singular values [34].The RCD technique leads to a better performance in low-SNR regimes, while for high SNR, the transmission tends to concentrate in the null-space of $\ddot{H}_k$, and therefore, the RCD precoder approaches the RBD design [28].

2.5. Water filling Power Allocation

Allocate the power according to the solution to the waterfilling problem [26],

$$\max_{P[m]} \sum_1^{N_S} \log(1 + P[m]_{N_S} \times diagonal[\mathrm{H}_{N_S}]) \tag{19}$$
$$\text{Subject to } \sum P[m]_{N_S} \leq P_T$$

whose solution is given by

$$\left[P_{N_S}\right] = (\partial - diagonal[\mathrm{H}_{N_S}]^{-1})^+ \tag{20}$$

where $\left[P_{N_S}\right] = diagonal\ [P[m]_1\ P[m]_2 \dots P[m]_{N_S}]$ is the power allocated to the N_S-th data stream in m-th subcarrier, H_{N_S} is the N_S-th diagonal of the effective channel $\mathrm{H}_{N_S} = F[m]_{BB} H[m]_{eff} W[m]_{BB}^H$, $(\partial)^+ \triangleq \max(0; \partial)$, and ∂ is the water level chosen to satisfy the transmitted power constraint. Therefore, the digital precoder is finally given by $F[m]_{BB} = P_{N_S} F[m]_{BB}$.

2.6. Computational complexity

In designing analog beamforming, the computational complexity order required is $KN_S N_T N_R[N_{it} + K]$, where N_{it} is the number of iterations needed to compute an analog beamforming vector pair. The digital beamforming design needs the computation of the effective baseband channel; with complexity order of $[KN_S(N_T N_R + KN_T N_S)$. In SU systems, to design analog beamforming requires that computation complexity order of $[N_S N_T N_R N_{it}]$ and its computation complexity order of the effective baseband channel is reduced to $[N_S^2 N_T + N_S N_T N_R]$. The digital beamforming design is achieved from the effective baseband channel's SVD with complexity order of $[N_S^3]$, followed by the digital precoder normalization with complexity order of $[N_S^2 N_T]$ under the assumption that $N_S \leq N_T$ and $N_S \leq N_R$. In [27], the computational complexity order of designing SS-SVD HBF is $[MN_T(N_T^2 + N_S^2) + N_S(N_T^2 + N_R^2)]$. The SS-SVD design is expand from SU (i.e., $K = 1$) systems to MU (i.e.,$K \neq 1$) systems using combination of (MU-SS) algorithm for analog beamforming and (MU-SVD) algorithm for digital beamforming. Thus, the complexity order of using MU-SS and MU-SVD algorithms together can be derived as $K[MN_T(N_T^2 + N_S^2) + N_S(N_T^2 + N_S^2)]$. In MU systems, the digital beamforming design is achieved from the RCD

design with complexity order of $[K^4N_S^3]$, followed by the digital precoder normalization with complexity order of $[K^2N_S^2N_T]$ [28]. Therefore, under the assumption that $N_S \leq N_T$ and $N_S \leq N_R$. For comparison, the complexity orders of the existing HBF designs are presented in Table 1.

Table 1 Computational Complexity of SU and MU-MIMO HBF Design Methods

Methods	**Complexity orders**
MU-SS (Prop.) and MU-SVD	$K[MN_T(N_T^2 + N_S^2) + N_S(N_T^2 + N_S^2)]$
SS-SVD [14]	$MN_T(N_T^2 + N_S^2) + N_S(N_T^2 + N_R^2)$
FD-BD [18]	$K[K^3N_S^3 + KN_S^2N_T + N_TN_R^2]$
HRCD [19]	$K[K^3N_S^3 + KN_S^2N_T + N_TN_R^2 + N_SN_{cl}N_{ray}]$
DZhang2019 (TU-HBF) [31]	$MK(K^3N_S^3 + N_T^2N_S + KN_TN_R^2 + N_S^2N_R)$

3. Simulation Results and discussion

In the simulation setup, a communication bandwidth of W = 0.5GHz centered over the carrier frequency f_C = 28GHz is considered. This section presents numerical results to assess the effectiveness of the SS-RCD and the SS-BD compares its performance with other existing HBF designs. We consider a Saleh Valenzuela channel model with $N_{ray} = 10$ propagation paths per cluster and $N_{cl} = 5$ scattering clusters, a USPA with antenna spacing $d = \lambda/2$, and angular spread $\sigma_{\varphi}^{T} = \sigma_{\varphi}^{R} = \sigma_{\vartheta}^{T} = \sigma_{\vartheta}^{R} = 10^{o}$. We define SNR at mobile user as SNR = $\rho\frac{P_T}{\sigma^2}$ and consider total transmit Power, $P_T = KN_S$. For simplicity, we consider that all users to have the same SNR. We present the performance results for both SU and MU systems. A detailed description of the simulation parameters is reported in table 2. The results presented come from an average over 100 independent realizations of propagation channels.

Table 2 System parameters

Description	**Value**
Carrier frequency	f_C = 28GHz
Bandwidth	W = 0.5GHz
BS antenna array	USPA With λ /2 spacing
User antennas	USPA With λ /2 spacing

We consider the uniform power allocation that is the N_S-dimensional diagonal matrix containing the power allocation is

$$P_k = diag(\frac{P_T}{N_S}, \dots, \frac{P_T}{N_S}) \; For\ all\ k = 1 \dots K. \tag{21}$$

where P_k is the power allocated to k-th user.

3.1. SU Systems

The SS-BD is compared with the optimal unconstrained beamforming, the Sohrabi2017 (HBF-LSAA) [10–11], PE-AltMin [13], SS-SVD [14], ICSI-HBF [29] (considering an orthogonal codebook with C = 64), and the PE-HOSVD [30] for SU-OFDM systems (i.e. K = 1) with M = 32 subcarriers. We assume a system with a symmetrical communication is considered ($N_T = N_R = 64$ antennas) and $N_T^{RF} = N_F^{RF} = N_S$ RF chains communicating via N_S = 4 data streams per subcarrier in all the experiments.

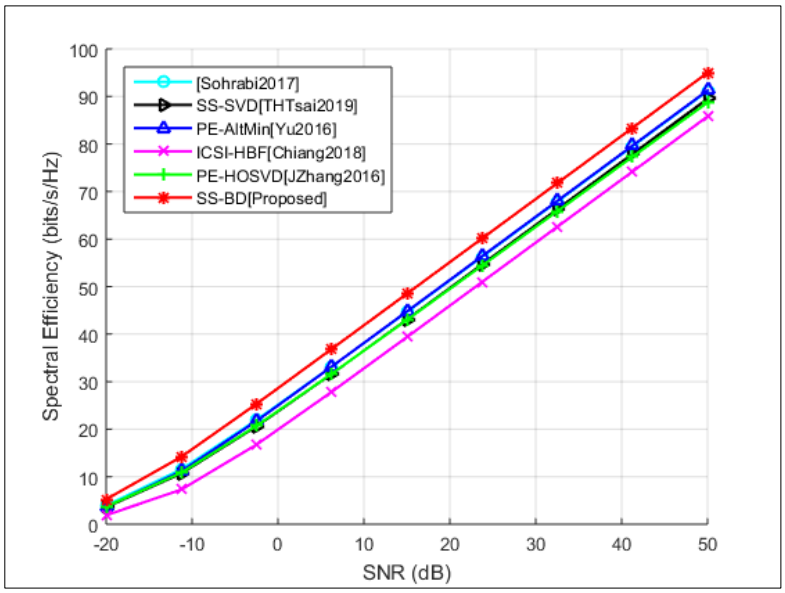

Figure 2 Average spectral efficiency vs. SNR for a SU system with $\boldsymbol{N_T = 64, N_R = 64, N_S = 4}$ & $\boldsymbol{M = 32}$.

The first experiment investigates the impact of the SNR on the spectral efficiency. The results, shown in figure 2, illustrate that the SS-BD design marginally outperforms other designs over all SNR range and obtains near-optimal performance in terms the spectral efficiency. The SS-BD achieves spectral efficiency, on average, 2.84 bits/s/Hz higher than the PE-AltMin and Sohrabi2017 (HBF-LSAA) designs, and 3.78 bits/s/Hz higher than the SS-SVD and PE-HOSVD at SNR = 15 dB, while ICSI-HBF has the least performance and especially at low SNR (less than -10dB). The performance gap between SS-SVD and PE-HOSVD designs is negligible. However, ICSI-HBF and PE-HOSVD have lower spectral efficiency due to decreased solution space for the analog combiner and precoder design problems.

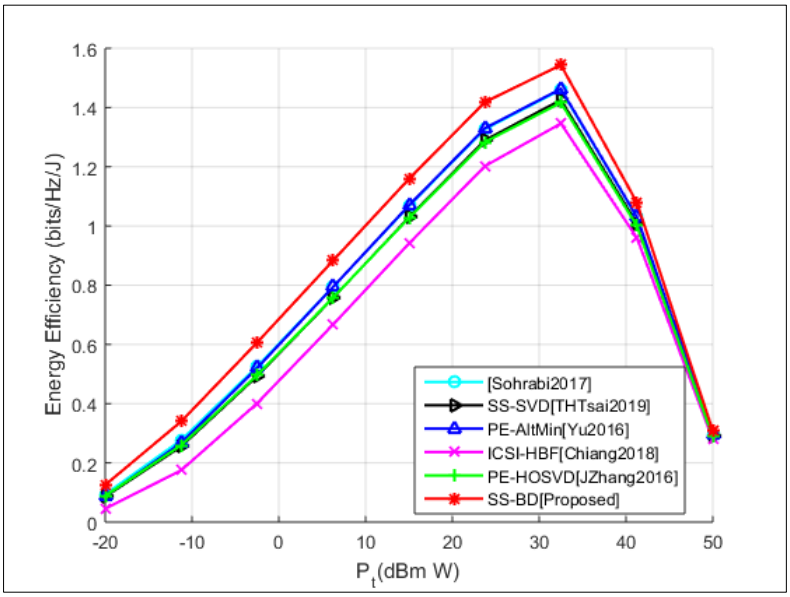

Figure 3 Average energy efficiency vs. transmit Power ($\boldsymbol{P_T}$) for a SU system with $\boldsymbol{N_T = 64, N_R = 64, N_S = 4}$ & $\boldsymbol{M = 32}$ at SNR = -5dB.

The second experiment evaluates the impact of the transmit Power (P_T) on the energy efficiency performance. We assume a system with $N_T = N_R = 64$ antennas and $N_T^{RF} = N_F^{RF} = N_S$ RF chains communicating via $N_S = 4$ data streams per subcarrier for SNR of -5dB. The results, shown in Fig. 3, one can observe that the SS-BD marginally outperforms other designs over all P_T range. The SS-BD method achieves energy efficiency, on average, 0.24 bits/s/Hz/J higher than the PE-AltMin and Sohrabi2017 (HBF-LSAA) designs, and 0.35bits/s/Hz/J higher than the SS-SVD and PE-HOSVD, while ICSI-HBF has the least energy efficiency performance among the designs at P_T = 32.67dBm W. The SS-BD method achieves a higher energy efficiency, since it can obtain the near-optimal spectral efficiency while needing substantially

low power consumption as presented above. Besides, one can observe that there exists an optimal system energy efficiency operating point (P_T = 32.67dBm W). Such behavior can be interpreted as follows. When the P_T is relatively small, increasing the P_T results in a higher energy efficiency since the total power consumption is dominated by the circuit power consumption i.e., P_{RFC} and P_{BB} in (7b) and (7c). Moreover, when the P_T is sufficiently bigger than other terms in the power consumption model i.e., P_T = 32.67dBm W, increasing P_T will decrease energy efficiency instead.

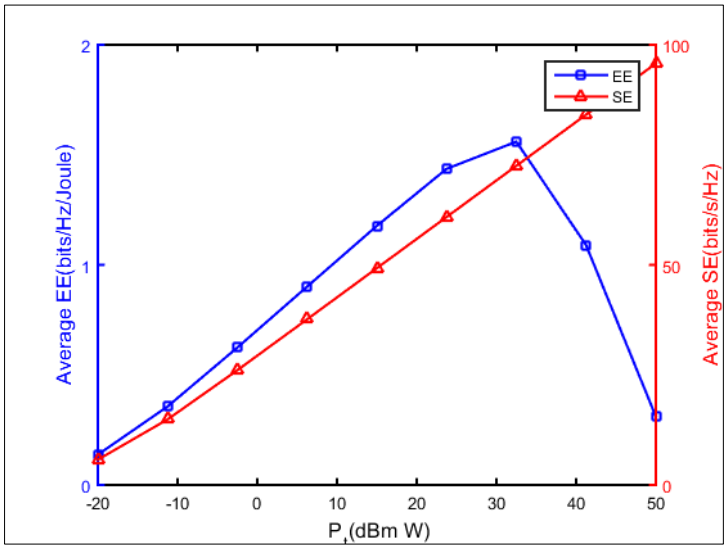

Figure 4 Average EE and SE vs. transmit Power ($\boldsymbol{P_T}$) for a SU system using SS-BD method with $\boldsymbol{N_T = 64, N_R = 64, N_S = 4}$ & $\boldsymbol{M = 32}$ at SNR = -5dB.

The impact of transmit Power (P_T) on the average energy efficiency (EE) and spectral efficiency (SE) performances for the SS-BD HBF is depicted in figure 4, we can observe that the excessive increase in P_T (> 32.67 dBm W) leads to deterioration in energy efficiency and growth in spectral efficiency. This could be explained by the fact that the P_T contributes to the total power consumption in a linear manner, while it contributes to the energy efficiency and spectral efficiency in a logarithm manner.

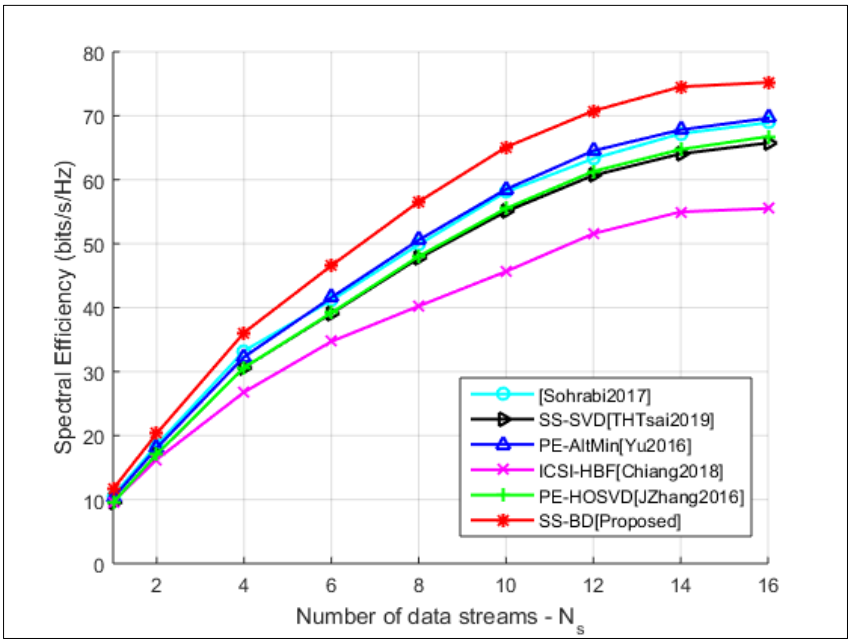

Figure 5 Average spectral efficiency vs. number of data streams ($\boldsymbol{N_S}$) for a SU system with $\boldsymbol{N_T = 64, N_R = 64, N_S = 4}$ & $\boldsymbol{M = 32}$ at SNR = -5dB.

The impact of the data streams (N_S) on the spectral efficiency is evaluated in this experiment. The results shown in Fig. 5, present that the SS-BD method considerably outperforms other designs over all N_S range. The SS-BD method achieves spectral efficiency, on average, 6.13 bits/s/Hz higher than the PE-AltMin and (HBF-LSAA) designs, and 10.2 bits/s/Hz higher than the SS-SVD and PE-HOSVD designs when N_S = 16, while ICSI-HBF has the least performance. The SS-BD method has optimal performance especially when there is a high number of data streams transmitted.

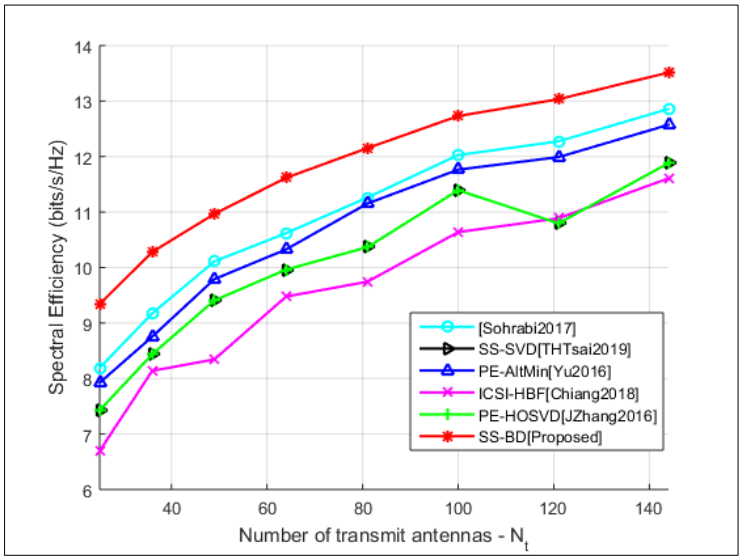

Figure 6 Average spectral efficiency vs. N_T for a SU system with $N_T = N_R, N_S = 4$ & $M = 32$ at SNR = -5dB.

This experiment evaluates the impact of the number of antennas (N_T) on the spectral efficiency. We assume a SU-OFDM system with $M = 32$, $N_T = N_R$ antennas and $N_T^{RF} = N_F^{RF} = N_S$ RF chains communicating via N_S = 4 data streams per subcarrier. The results shown in fig. 6, present that the SS-BD method greatly outperforms other designs over all N_T range. The SS-BD design has the highest spectral efficiency for any N_T and passes from 9.18bits/s/Hz to 13.50 bits/s/Hz as the N_T increases, while other designs follow the same trend. The SS-BD method achieves spectral efficiency, on average, 0.9 bits/s/Hz higher than the Sohrabi2017 (HBF-LSAA) and PE-AltMin, and 1.7 bits/s/Hz higher than the SS-SVD and the PE-HOSVD designs at N_T = 140. The spectral efficiency performance gap between SS-SVD and PE-HOSVD designs is zero. In addition, one can see that the PE-AltMin design can obtain the highest spectral efficiency in nearly all the experiments.

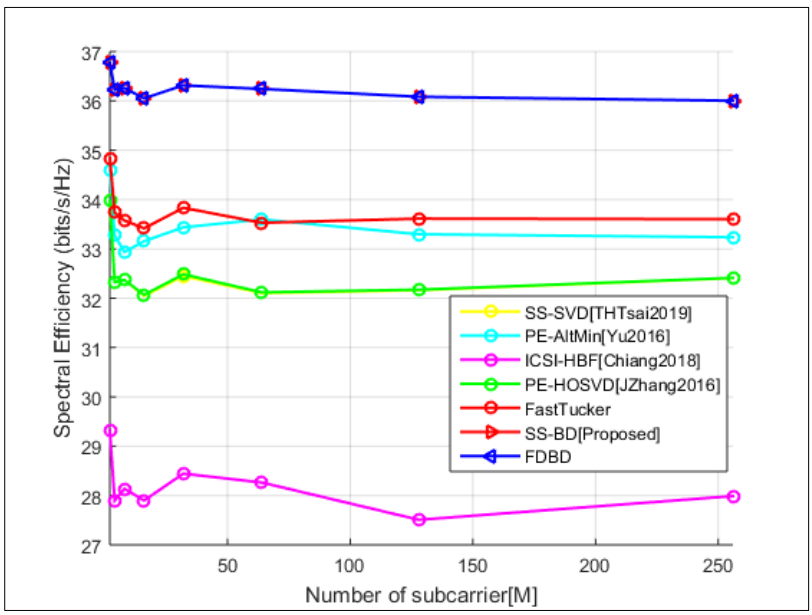

Figure 7 Average spectral efficiency vs. number of subcarrier (M) for a SU system with $N_T = 64, N_R = 64, N_S = 4$ & $M = 32$ at SNR = -5dB.

This experiment evaluates the impact of the number of subcarrier (M) on the spectral efficiency. We consider a SU-OFDM system with $N_T = N_R$ antennas and $N_T^{RF} = N_R^{RF} = N_S$ = 4 RF chains communicating via N_S = 4 data streams. In figure 7, FDBD and SS-BD designs have the highest spectral efficiency values among other designs. FastTucker [27-28] and PE-AltMin have the second best performance; PE-HOSVD and SS-SVD have the third best performance while ICSI-HBF has the least performance. By inspection, we observe that large M does not affect the spectral efficiency. In practical situations, OFDM systems often make use of larger numbers of subcarriers (i.e., $M \geq 128$) [27-28]. We have decided to limit our analysis to $16 \leq M \leq 32$ because of the computational time of the HBF designs.

3.2. MU Systems

This section evaluates the performance of the proposed method in MU-MIMO systems. The proposed design is compared with the MU-SVD (i.e., Algorithm 2), fully digital regularized block diagonalization (FD-RDB) [17], fully digital block diagonalization (FD-BD) [18], BeamformingRCD [28], DZhang2019 (TU-HBF) [31], and Gonzalez2018 (HD-PG-MMSE) [32]. The MU-SVD is the equivalent of the SS-SVD HBF design for MU. The FD-RDB design is used as a fully-digital benchmark, as it gives better performance than the conventional FD-BD. However, note that the MU-SVD is not capacity-achieving, and hybrid beamforming designs may outperform the fully-digital design in some situations. Moreover, the hybrid-RCD (HRCD) design [19] requires the knowledge of the array response vectors for all propagation paths and can only be deployed for the mmWave channel model. However, note that the fully-digital RCD is also suboptimal and thus, in some conditions, HBF designs may exceed its performance. In all experiments, we have considered an OFDM system with either M = 16 or M = 32 subcarriers. In SU systems, a symmetrical communication is assumed, while in MU systems, an asymmetrical communication ($N_T = 144$ & $N_R = 16$) is considered. Inspecting the figures in MU system, it is seen that the best performing beamforming structure is the SS-RCD method, both in terms of energy efficiency and of spectral efficiency excluding FD-RDB and FD-BD designs. This signifies that the growth in system spectral efficiency given by the SS-RCD beamforming structure, which nulls the noise and interference. FD-RBD and FD-BD designs give excellent performance in terms of simultaneously transmission, are not well compensated by the reduction of the power consumption in the MU-SVD structure.

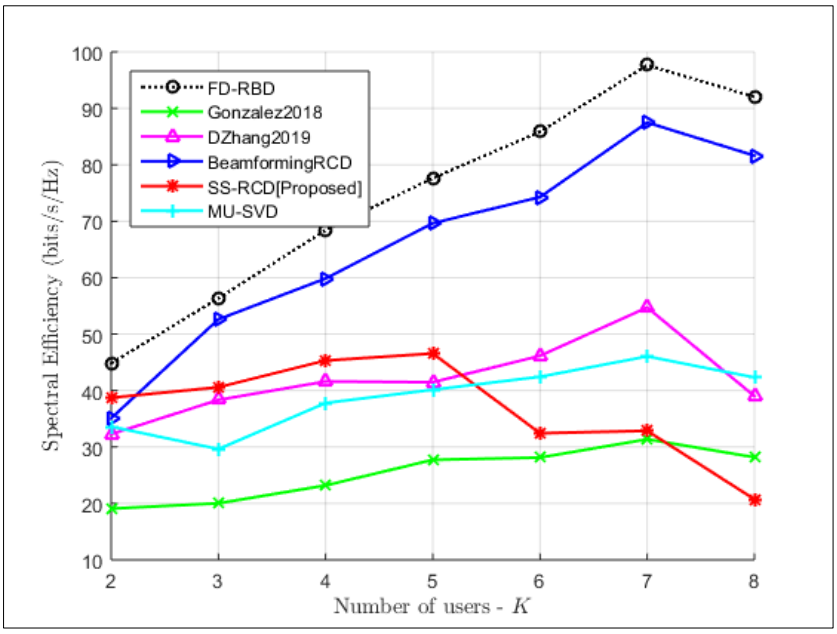

Figure 8 Average spectral efficiency vs. number of users ($\boldsymbol{K}$) for a MU system with $\boldsymbol{N_T = 144, N_R = 9, N_S = 4}$ & $\boldsymbol{M = 16}$ at SNR = -5dB.

The impact of the number of users (K) on the spectral efficiency was carried out in this experiment. We consider a MU-OFDM system with N_S = 4 data streams, $M = 16$ subcarriers, $N_T = 144$ and $N_R = 9$ antennas. The results, illustrated in figure 8, depict that FD-RDB and BeamformingRCD greatly outperform the other HBF designs. The SS-RCD method slightly performed better than DZhang2019 (TU-HBF), MU-SVD and Gonzalez2018 (HD-PG-MMSE) from K = 2 to K = 5 attaining spectral efficiency ranging from 38.22bits/s/Hz to 46.56 bits/s/Hz and has its performance deteriorated with the increase in the number of users, particularly at K > 5.

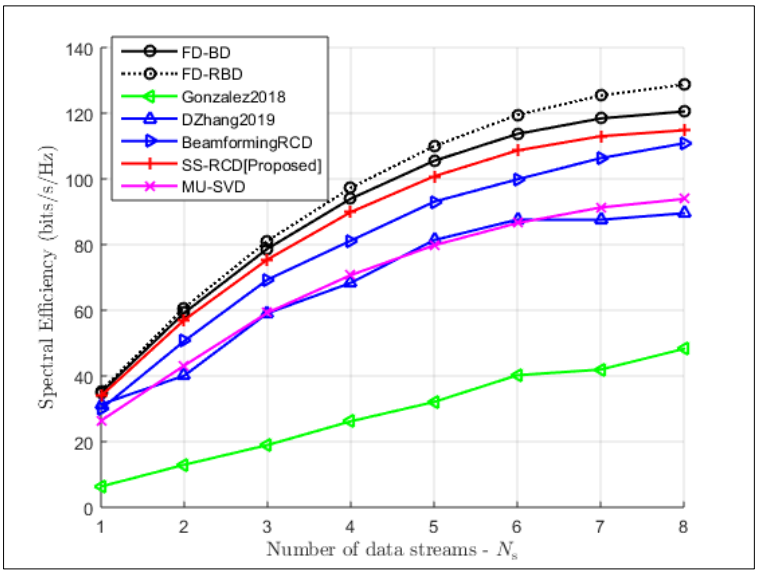

Figure 9 Average spectral efficiency vs. number of streams $\boldsymbol{N_S}$ for a MU system with $\boldsymbol{K = 4, N_T = 144, N_R = 16, N_S = 4}$ & $\boldsymbol{M = 32}$ **at SNR** $\boldsymbol{= -5}$**dB**.

The impact of the number of streams (N_S) on the spectral efficiency was evaluated in this experiment. We consider a MU-OFDM system with K = 4 users, $M = 32$ subcarriers, SNR = -5dB, $N_T = 144$ and $N_R = 32$ antennas. In particular in Figure 9, we can see that the performance in terms of spectral efficiency of DZhang2019 (TU-HBF) and MU-SVD are very close, while the performance of the Gonzalez2018 (HD-PG-MMSE) is very poor. The SS-RCD has considerably better performance than other HBF designs excluding FD-RDB and FD-BD methods, attaining around 4.2 bits/s/Hz higher spectral efficiency than the BeamformingRCD and 20.86 bits/s/Hz higher spectral efficiency than MU-SVD and DZhang2019 (TU-HBF) at $N_S = 8$, respectively. Interestingly, the spectral efficiency of the proposed method (SS-RCD) is 2.5 times higher than with the Gonzalez2018 (HD-PG-MMSE).We can see that increase in N_S enhances the growth of HBF designs' spectral efficiency.

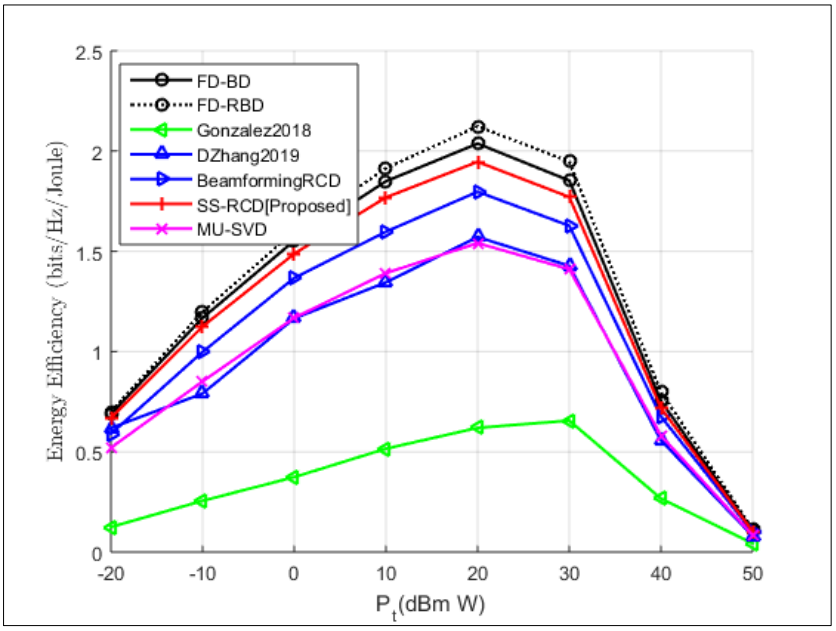

Figure 10 Average energy efficiency vs. transmit Power ($\boldsymbol{P_T}$) for a MU system with $\boldsymbol{K = 4, N_T = 144, N_R = 9, N_S = 4}$ & $\boldsymbol{M = 16}$ at SNR = -5dB.

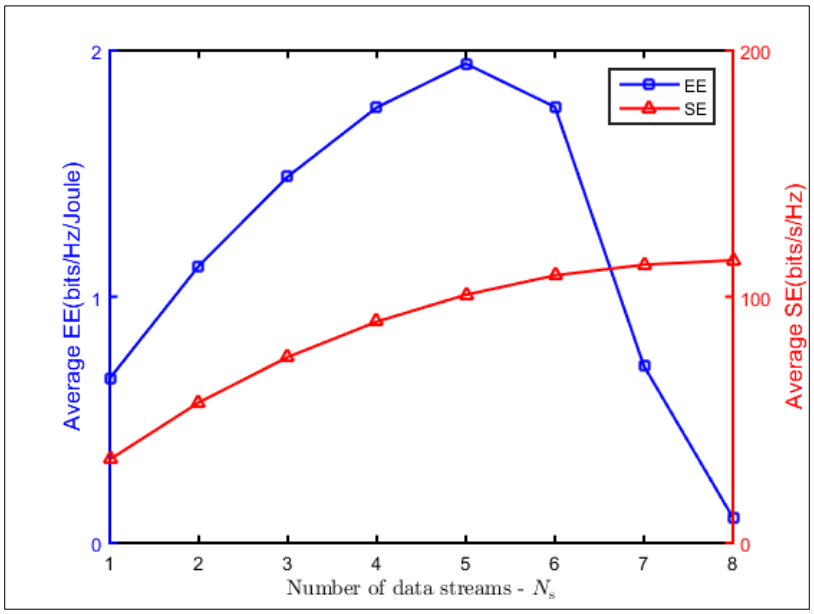

Figure 11 Average EE and SE vs. number of data streams ($\boldsymbol{N_S}$) for a MU system using SS-SCD with $\boldsymbol{K = 4, N_T = 144, N_R = 32, N_S = 4}$ & $\boldsymbol{M = 32}$ at SNR = -5dB.

The impact of the transmit power (P_T) on the energy efficiency was evaluated in this experiment. We consider a MU-OFDM system with $K = 4$ users, $M = 16$ subcarriers, SNR = -5dB, $N_T = 144$ and $N_R = 9$ antennas. Focusing on the energy efficiency performance, one can see that the reduction of the power consumption in the HBF designs gives an increase in terms of energy efficiency, while the decrease of power consumption in the Gonzalez2018 (HD-PG-MMSE) method cannot compensate the gap in terms of SE with the SS-RCD beamforming, while the spectral efficiency grows with the transmit power ($P_T = KN_S$) at least in the considered range of values, the energy efficiency exhibits instead a maximum around 20 dBmW in figure 10. This behavior is best explained by the fact that for large values of the P_T, the numerator in the energy efficiency increase; at a slower rate than the denominator of the energy efficiency, and so the energy efficiency itself decreases. From an energy-efficient perspective, raising the P_T beyond the energy efficiency-optimal point leads to moderate improvements in the system throughput at the price of a much higher growth in the consumed power. Additionally, one can see that there is a region where both spectral efficiency and energy efficiency increase.

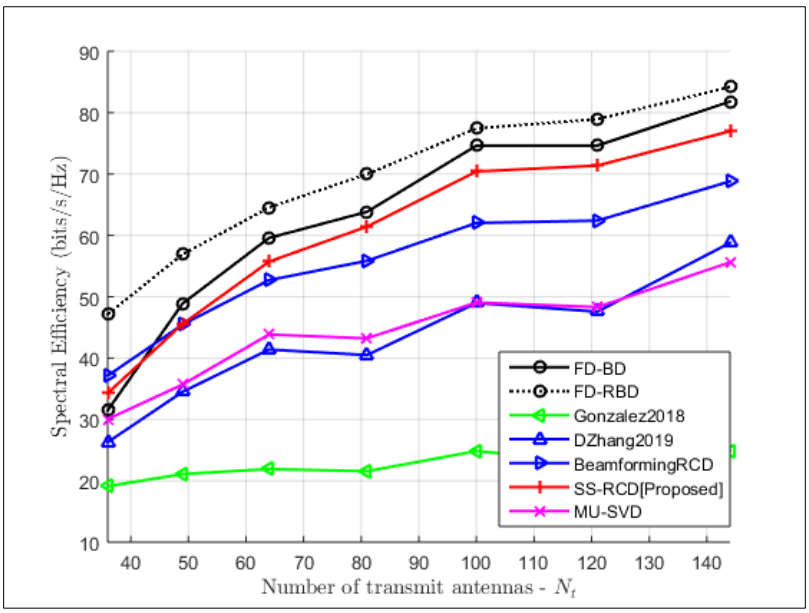

Figure 12 Average spectral efficiency vs. number of antennas ($\boldsymbol{N_T}$) for a MU system with $\boldsymbol{K = 4, N_R = 16, N_S = 4}$ & $\boldsymbol{M = 32}$ at SNR = -5dB.

In figure 11, SS-SCD method has its energy efficiency performance deteriorated with the increase in the number of data streams, particularly at optimal point $N_S \geq 5$ because the data streams is proportional to the transmit power, $P_T = KN_S$ while spectral efficiency has a steady increase with N_S.

The impact of the number of transmit antennas (N_T) on the spectral efficiency was evaluated in this experiment. We assume a MU-OFDM system with K = 4 users, $M = 32$ subcarriers, SNR = -5dB, and $N_R = 32$ antennas. Figure 12 presents the results, showing that the performance in terms of spectral efficiency of MU-SVD and DZhang2019 (TU-HBF) are very close, while the Gonzalez2018 (HD-PG-MMSE) performed very poorly. SS-RCD has the third best performance and considerably outperforms other HBF methods excluding FD-RDB and FD-BD designs, having around 9.4 bits/s/Hz higher spectral efficiency than the BeamformingRCD and 17.24 bits/s/Hz higher spectral efficiency than both the DZhang2019 (TU-HBF) and the MU-SVD designs at $N_T = 144$, respectively. The suboptimal designs are quite competitive when N_T is small. Interestingly, the spectral efficiency of the SS-RCD design is 3.5 times higher than with the Gonzalez2018 (HD-PG-MMSE) design, which passes from 35.12bits/s/Hz to 78.230 bits/s/Hz as the N_T increases. We can see that increase in N_T boosts the HBF designs' spectral efficiency.

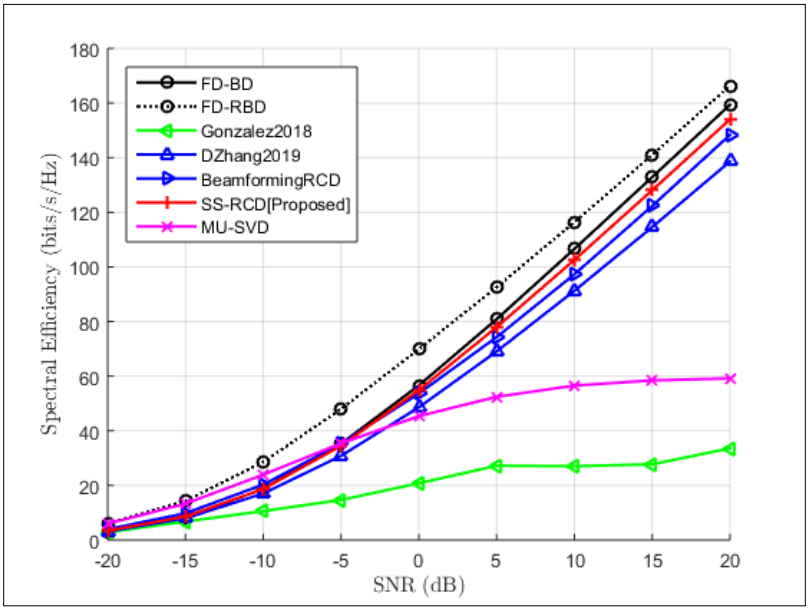

Figure 13 Average spectral efficiency vs. SNR for a MU system with $\boldsymbol{K = 4, N_T = 144, N_R = 16, N_S = 4}$ & $\boldsymbol{M = 32}$.

The impact of the number of SNR on the spectral efficiency was investigated in this experiment. We assume a MU-OFDM system with K = 4 users, M = 32, subcarriers, $N_T = 144$ and $N_R = 16$ antennas. Figure 13 depicts the results, showing again that the SS-RCD has the third best spectral efficiency performance and considerably marginally outperforms other HBF methods excluding FD-RDB and FD-BD designs, attaining around 5.30 bits/s/Hz higher spectral efficiency than the BeamformingRCD and 12.23 bits/s/Hz higher spectral efficiency than the DZhang2019(TU-HBF) design at SNR = 5dB, respectively. Gonzalez2018 (HD-PG-MMSE) method had least performance among HBF designs. However, at low SNR that is SNR < 5dB, the MU-SVD method slightly outperformed other methods excluding FD-RBD method. Nevertheless, despite the slightly better performance of the MU-SVD method in low-SNR scenarios, its performance is severely deteriorated in high SNR.

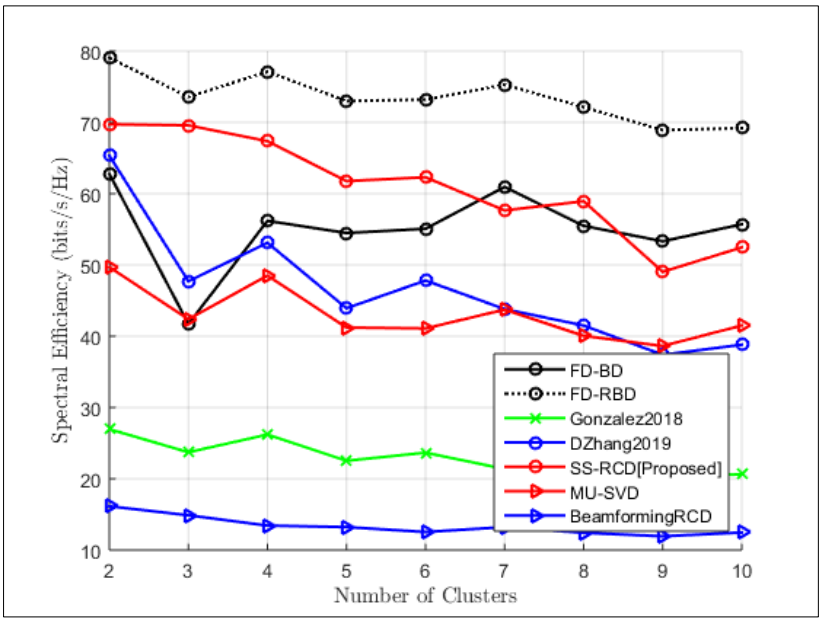

Figure 14 Average SE vs. number of scattering clusters for a MU system with $N_T = 72, N_R = 16, N_S = 4$ & $M = 16$ at SNR = -5dB.

The impact of the number of scattering clusters on the SE was evaluated in this experiment. We assume a MU system with K = 4 users, $M = 16$ subcarriers, SNR = -5dB, $N_T = 72$ and $N_R = 16$ antennas. With the increase of the number of the scattering clusters, the MUI and the IUI are enhancing. Although the performance of FD-RBD and SS-RCD methods are good, while Gonzalez2018 (HD-PG-MMSE) and BeamformingRCD methods have performance degradation.

Both MU-SVD and DZhang2019 (TU-HBF) designs have a moderate performance. This confirms the superiority of the SS-RCD in reducing the MUI noise.

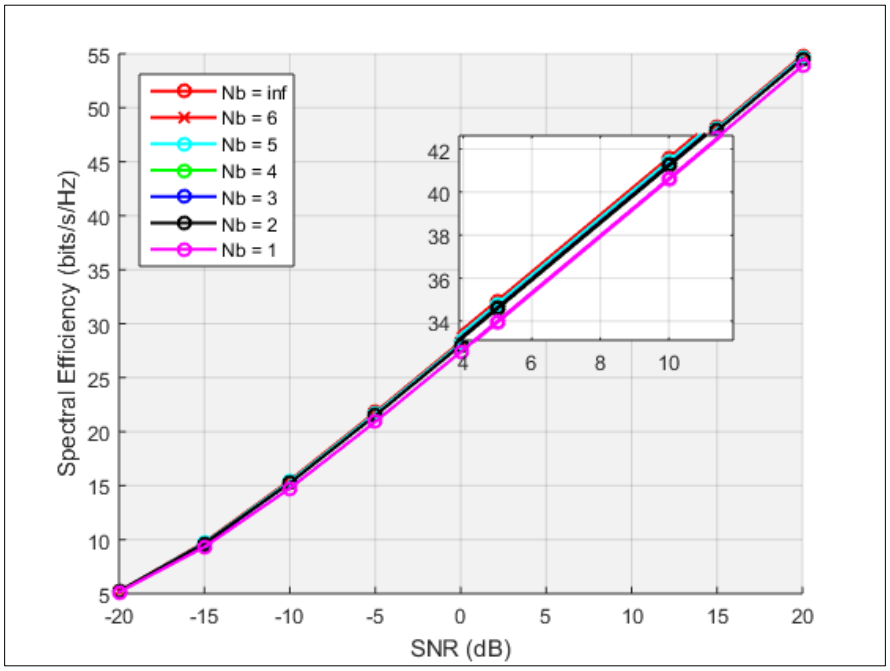

Figure 15 Average spectral efficiency attained by the quantized SS-RCD vs. SNR for different quantization bits (N_b) at SNR = -5 dB.

The impact of the SNR for different quantization bits (N_b) on the spectral efficiency attained by the quantized SS-RCD was investigated in this experiment. The results obtained in figure 15, show that the un-quantized ($N_b = \infty$) marginal outperformed other quantization bits (N_b).

4. Discussions

The numerical results shown above have illustrated that the SS-RCD design consistently outperforms the other design methods in nearly all mmWave scenarios. In particular, the SS-RCD and SS-BD methods provide significant improvement in energy and spectral efficiency performance. Such an improvement is due to interference suppression at the digital beamforming and capacity to harvest array gain at the analog beamforming. Moreover, simulation results have also illustrated the performance under practical constraints, such as the quantized phase shifter implementation of the analog beamforming the computational complexity of our design is similar to other existing methods.

5. Conclusion

In this paper, we proposed a hybrid beamforming design for single-user and multi-user mmWave massive MIMO-OFDM systems and have presented some relevant use cases, focusing on energy and spectral efficiency problems. The proposed method consists of a two-step method in which we design the analog and digital beamforming separately. The analog precoder and combiner design is based on a SS method, which aims to maximize the array gain given by the massive MIMO system while nulling the effect of interference. In the second step, the digital beamformers are computed using the RCD and BD solutions for multi-user and single-user respectively. The solutions provide interference suppression and more transmit diversity, therefore obtaining higher performances when the number of mobile users, antennas and streams are increased. Numerical results have confirmed the effectiveness of our design, which outperforms other existing designs.

Compliance with ethical standards

Acknowledgments

Special thanks to Dr. Ahaneku M. A. for his guidance, supports and contributions towards the actualization of this paper.

Disclosure of conflict of interest

There was no conflict of interest.

References

[1] I F Akyildiz, A Kak, and S Nie. 6G and beyond: the future of wireless communication systems. IEEE Access. 2020; 8(1):133995–134030.

[2] M Giordani, M Polese, M Mezzavilla, S Rangan, and M Zorzi. Toward 6G networks: use cases and technologies. IEEE Communications Magazine. 2020; 58(3):55–61.

[3] Q Bi. Ten trends in the cellular industry and an outlook on 6G. IEEE Communication Magazine. 2019; 57(12): 31–36.

[4] T S Rappaport et al. Millimeter wave mobile communications for 5G cellular: it will work!. IEEE Access. 2013; 1(1):335–349.

[5] A A Nasir, H D Tuan, T Q Duong, H V Poor, and L Hanzo. Hybrid beamforming for multi-user millimeter-wave networks. IEEE Transaction Vehicular Technology. 2020; 69(3):2943–2956.

[6] I Ahmed, H Khammari, A Shahid, A Musa, K S Kim, E De Poorter, and I Moerman. A survey on hybrid beamforming techniques in 5G: architecture and system model perspectives. IEEE Communications Surveys Tutorial. 2018; 20(4):3060–3097.

[7] M Rihan, T A Soliman, C Xu, L Huang, and M I Dessouky. Taxonomy and performance evaluation of hybrid beamforming for 5G and beyond systems. IEEE Access. 2020; 8(1):74605–74626.

[8] J Zhang, X Yu, and K B Letaief. Hybrid beamforming for 5G and beyond millimeter-wave systems: a holistic view. IEEE O J Communications Society. 2020; 1(1):77–91.

[9] Xue X, Wang Y, Yang L, Shi J, and Li Z. Energy-efficiency hybrid precoding for massive MIMO mmWave systems with a fully adaptive-connected structure. IEEE Transaction Communications. 2020; 68(6):3521–3535.

[10] Sohrabi F and Yu W. Hybrid Analog and Digital Beamforming for mmWave OFDM Large-Scale Antenna Arrays. IEEE Journal on Selected Areas in Communications. 2017; 35(7):1432–1443. DOI:10.1109/JSAC.2017.2698958.

[11] Sohrabi F and Yu W. Hybrid digital and analog beamforming design for large-scale antenna arrays. IEEE Journal of Selected Topics in Signal Processing. 2016; 10(3):501–513. DOI: 10.1109/JSTSP.2016.2520912.

[12] A F Molisch, V V Ratnam, S Han, Z Li, S L H Nguyen, L Li, and K Haneda. Hybrid beamforming for massive MIMO: a survey. IEEE Communications Magazine. 2017; 55(9):134–141.

[13] X Yu, J-C Shen, J Zhang, and K B Letaief. Alternating minimization algorithms for hybrid precoding in millimeter wave MIMO systems. IEEE Journal Selection Topics Signal Processing. 2016; 10(3):485–500.

[14] T Tsai, M Chiu, and C Chao. Sub-system SVD hybrid beamforming design for millimeter wave multi-carrier systems. IEEE Transactions Wireless Communication. 2019; 18(1):518–531.

[15] J Du, W Xu, C Zhao, and L Vandendorpe. Weighted spectral efficiency optimization for hybrid beamforming in multiuser massive MIMO-OFDM systems. IEEE Transactions Vehicular Technology. 2019; 68(10): 9698–9712.

[16] Y Liu, and J Wang. Low-complexity OFDM-based hybrid precoding for multiuser massive MIMO systems. IEEE Wireless Communications Letters. 2020; 9 (3): 263–266.

[17] W Ni and X Dong, Hybrid block diagonalization for massive multiuser MIMO systems. IEEE Transactions Communication. 2016; 64(1): 201–211.

[18] R Rajashekar and L Hanzo. Iterative matrix decomposition aided block diagonalization for mm-Wave multiuser MIMO systems. IEEE Transactions Wireless Communications. 2017; 16(3): 1372–1384.

[19] F Khalid. Hybrid beamforming for millimeter wave massive multiuser MIMO systems using regularized channel diagonalization. IEEE Wireless Communications Letters. 2019; 8(3):705–708.

[20] C Kim, T Kim, and J Y Seol. Multi-beam transmission diversity with hybrid beamforming for MIMO-OFDM systems. Proc 2013 IEEE Globecom Work Atlanta, GA, USA. 2013:61–65.

[21] Stefano Buzzi and Carmen D' Andrea. Energy-efficient design for doubly massive MIMO millimeter wave wireless systems. In: Himal A Suraweera, Jing Yang, Alessio Zappone and John S Thompson. Green Communications for Energy-Efficient Wireless Systems and Networks. First edition London: The Institution of Engineering and Technology; 2021. p. 265–290

[22] E Björnson, L Sanguinetti, J Hoydis, and M Debbah. Optimal design of energy-efficient multi-user MIMO systems: Is massive MIMO the answer?. IEEE Transactions on Wireless Communications. 2015; 14(6):3059–3075.

[23] O E Ayach, S Rajagopal, S Abu-Surra, Z Pi, and R W Heath. Spatially sparse precoding in millimeter wave MIMO systems. IEEE Transactions on Wireless Communications. 2014; 13(3):1499-1513.

[24] X Yu, J-C Shen, J Zhang, and K B Letaief. Alternating minimization algorithms for hybrid precoding in millimeter wave MIMO systems. IEEE Journal of Selected Topics in Signal Processing. 2016; 10(3):485-500.

[25] G Raleigh and J Cioffi. Spatio-temporal coding for wireless communication. IEEE Transactions on Communications. 1998; 46(3):357-366.

[26] D Palomar and J Fonollosa. Practical algorithms for a family of watefilling solutions. IEEE Transactions on Signal Processing. 2005; 53(2):686-695.

[27] G M Zilli and W-P Zhu. Constrained-SVD based hybrid beamforming design for millimeter wave communications. In IEEE 92nd Vehicular Technology Conference VTC2020-Fall Victoria, BC, Canada. Nov. 2020.

[28] G M Zilli and W-P. Zhu. Constrained channel decomposition-based hybrid beamforming for mmWav massive MIMO systems. IEEE O J Communications. Society.2020; 1(1):1707–1720.

[29] H-L Chiang et al. Hybrid beamforming based on implicit channel state information for millimeter wave links. IEEE Journal Selection Topics Signal Processing. 2018; 12(2); 326–339.

[30] J Zhang, A Wiesel, and M Haardt. Low rank approximation based hybrid precoding schemes for multi-carrier single-user massive MIMO systems. In IEEE Int Conf Acoust Speech, Signal Processing 2016: 3281–3285.

[31] D Zhang, Y Wang, X Li, and W Xiang. Hybrid beamforming for downlink multiuser millimeter wave MIMO-OFDM systems. IET Communications. 2019; 13(11); 1557–1564.

[32] J P Gonzalez-Coma, J Rodriguez-Fernandez, N Gonzalez-Prelcic, L Castedo, and R W Heath. Channel estimation and hybrid precoding for frequency selective multiuser mmWave MIMO systems. IEEE Journal Selection Topics Signal Process. 2018; 12(2):353–367.

[33] Q Spencer, A Swindlehurst, and M Haardt. Zero-forcing methods for downlink spatial multiplexing in multiuser MIMO channels. IEEE Transactions on Signal Processing. 2004; 52(2):461–471.

[34] V Stankovic and M Haardt. Generalized design of multi-user MIMO precoding matrices. IEEE Transactions on Wireless Communications.2008; 7(3): 953–961.

[35] Zi R et al. Energy efficiency optimization of 5G radio frequency chain systems. IEEE Journal Selection Areas Communications 2016; 34(4): 758–771.